



## Organ chips with integrated multifunctional sensors enable continuous metabolic monitoring at controlled oxygen levels

Zohreh Izadifar<sup>a,1</sup>, Berenice Charrez<sup>a</sup>, Micaela Almeida<sup>a</sup>, Stijn Robben<sup>a,b</sup>, Kanoelani Pilobello<sup>a</sup>, Janet van der Graaf-Mas<sup>a</sup>, Susan L. Marquez<sup>a</sup>, Thomas C. Ferrante<sup>a</sup>, Kostyantyn Shcherbina<sup>a</sup>, Russell Gould<sup>a</sup>, Nina T. LoGrande<sup>a</sup>, Adama M. Sesay<sup>a</sup>, Donald E. Ingber<sup>a,c,d,\*</sup>

<sup>a</sup> Wyss Institute for Biologically Inspired Engineering, Harvard University, Boston, MA 02215, USA

<sup>b</sup> Department of Microelectronics, Technical University Delft, Delft, 2628 CD, Netherlands

<sup>c</sup> Vascular Biology Program and Department of Surgery, Harvard Medical School and Boston Children's Hospital, Boston, MA 02115, USA

<sup>d</sup> Harvard John A. Paulson School of Engineering and Applied Sciences, Harvard University, Cambridge, MA 02138, USA

### ARTICLE INFO

#### Keywords:

Organ-on-a-chip  
Sensor  
Oxygen  
pH  
Trans epithelial electrical resistance  
Metabolic sensing

### ABSTRACT

Despite remarkable advances in Organ-on-a-chip (Organ Chip) microfluidic culture technology, recreating tissue-relevant physiological conditions, such as the region-specific oxygen concentrations, remains a formidable technical challenge, and analysis of tissue functions is commonly carried out using one analytical technique at a time. Here, we describe two-channel Organ Chip microfluidic devices fabricated from polydimethylsiloxane and gas impermeable polycarbonate materials that are integrated with multiple sensors, mounted on a printed circuit board and operated using a commercially available Organ Chip culture instrument. The novelty of this system is that it enables the recreation of physiologically relevant tissue-tissue interfaces and oxygen tension as well as non-invasive continuous measurement of transepithelial electrical resistance, oxygen concentration and pH, combined with simultaneous analysis of cellular metabolic activity (ATP/ADP ratio), cell morphology, and tissue phenotype. We demonstrate the reliable and reproducible functionality of this system in living human Gut and Liver Chip cultures. Changes in tissue barrier function and oxygen tension along with their functional and metabolic responses to chemical stimuli (e.g., calcium chelation, oligomycin) were continuously and non-invasively monitored on-chip for up to 23 days. A physiologically relevant microaerobic microenvironment that supports co-culture of human intestinal cells with living *Lactococcus lactis* bacteria also was demonstrated in the Gut Chip. The integration of multi-functional sensors into Organ Chips provides a robust and scalable platform for the simultaneous, continuous, and non-invasive monitoring of multiple physiological functions that can significantly enhance the comprehensive and reliable evaluation of engineered tissues in Organ Chip models in basic research, preclinical modeling, and drug development.

### 1. Introduction

Organ-on-a-Chip (Organ Chip) technology offers immense potential for revolutionizing biomedical research, drug development, and personalized medicine by enabling the *in vitro* study of human organ-level physiology and disease states (Ingber, 2022). By recreating intricate tissue-tissue interfaces and precisely controlling the tissue microenvironment, Organ Chips bridge the gap between traditional cell culture and complex *in vivo* systems. However, widespread adoption of

this technology in research, preclinical, and clinical applications is hampered by challenges in establishing and maintaining physiological microenvironments on-chip, particularly due to the lack of non-invasive, real-time monitoring tools for multiple microenvironmental parameters and cellular responses.

Current monitoring methods for Organ Chips primarily rely on microscopic imaging or endpoint analysis such as cell viability, proliferation, protein secretion, gene expression, or metabolic changes (Ferrari et al., 2020; Fuchs et al., 2021), providing limited information

\* Corresponding author.

E-mail address: [don.ingber@wyss.harvard.edu](mailto:don.ingber@wyss.harvard.edu) (D.E. Ingber).

<sup>1</sup> Current address: Department of Urology, Boston Children's Hospital, Boston, MA 02115.

<https://doi.org/10.1016/j.bios.2024.116683>

Received 17 May 2024; Received in revised form 12 August 2024; Accepted 16 August 2024

Available online 17 August 2024

0956-5663/© 2024 The Authors. Published by Elsevier B.V. This is an open access article under the CC BY-NC license (<http://creativecommons.org/licenses/by-nc/4.0/>).

about the local intact tissue or dynamic tissue microenvironment. Advancements in miniaturized sensors offer promising solutions (Baracu and Dinu Gugoasa, 2021; Chauhan et al., 2021; Pfeiffer et al., 2017), however, integrating these sensors into Organ Chips while preserving tissue-level complexity and functionality, as well as allowing multiplexing and automation, remain a significant hurdle (Fuchs et al., 2021). Moreover, most sensor integrated chips are designed for use by the investigators who developed the technology and they are often complex and difficult to adapt for broader use.

Another critical challenge is recreating the physioxic (normal physiological oxygen) conditions found in most human tissues and organs (4.5–7% oxygen), which significantly influence cellular physiology and pathophysiology (Gan and Ooi, 2020). The high gas permeability of commonly used polydimethylsiloxane (PDMS) chip materials exacerbates this issue, as constant exposure to ambient air prevents the establishment of stable low oxygen levels. Existing methods for achieving physioxia in Organ Chips such as perfusion of anoxic medium through the one channel of a two-channel chip (Shin et al., 2019), culturing chips in anaerobic chambers while perfusing oxygenated medium through one of two channels (Jalili-Firoozinezhad et al., 2019) or wrapping portions of the PDMS chips in low gas permeable films (Grant et al., 2022) are labor-intensive, technically challenging, and often ineffective for long-term cultures.

To address these limitations, we developed a multifunctional sensor-integrated Organ Chip (siChip) system that combines a highly gas permeable PDMS with a low permeable polycarbonate (PC) material to maintain stable physiological oxygen levels without external intervention. By integrating multiple electrical and chemical sensors, as well as molecular reporters of cell metabolic activity (ATP/ADP), the siChip enables non-invasive, real-time monitoring of critical microenvironmental parameters and cellular responses. The siChip is designed to be mounted on a printed circuit board (PCB) and have a compact and versatile design to provide remote non-invasive sensing and to be easily integrated into a commercial Organ Chip culture system (Zoë™ Culture Module; Emulate Inc.) for scalability and automation.

We validated the siChip system using human Gut and Liver siChip models and demonstrated its ability to maintain stable oxygen levels within the physiological range (5–7%) on-chip based on the effects of cellular respiration and the ability of the PC walls of the chip to prevent oxygen transfer. We monitored key parameters of the tissue microenvironment, including oxygen levels, pH, cell metabolic activity (ATP/ADP ratio), and transepithelial electrical resistance (TEER) which provides a measure of tissue barrier integrity. Measurements were carried out continuously over long times (days to weeks) in the living chip cultures under baseline conditions and in response to different chemical stimuli (e.g., oligomycin, calcium chelator) as well as when human intestinal cells were co-cultured with living *Lactococcus lactis* bacteria.

## 2. Materials and methods

### 2.1. Design and fabrication of the sensor-integrated chip (siChip)

The microfluidic design of the siChip replicates the configuration of the commercial dual-channel Organ Chip device (Chip-S1; Emulate Inc. USA) to allow its incorporation with a portable module reservoir (Pod™; Emulate Inc.) that contains chambers for storing and collecting the chip media and effluents, respectively. This is accomplished by incorporating a microfluidic compartment that seamlessly connects the reservoirs to the chip enabling automated culture using a commercial culture module (Zoë™ Culture Module; Emulate Inc.) (Supplementary Figs. S1A and B). Like the Chip-S1, the dual-channel microfluidic siChip contains two parallel microchannels (1 mm wide × 1 mm high apical channel and a 1 mm wide × 0.2 mm high basal channel) separated by a porous membrane (50 μm thickness, 7 μm pores with 40 μm spacing) (Huh et al., 2013) for co-culturing two cell types, recreating tissue-tissue interfaces, and forming air-liquid or liquid-liquid flow interfaces on-chip. Hollow

chambers are located on both sides of the dual channel to which cyclic vacuum can be applied to physically distort the porous membrane and attached tissue-tissue interface and thereby mimic physiological mechanical deformations experienced within whole living organs *in vivo* (e.g., due to breathing, peristalsis, blood pressure pulses, etc.) (Supplementary Fig. S1A).

The dual-channel siChip was fabricated by assembling five different layers: apical and basal PDMS layers; apical and basal PC walls patterned with electrodes (for TEER measurements) and oxygen sensors (for oxygen tension measurements), and a PDMS porous membrane that separates the apical and basal channels on which different tissue-derived cells are cultured on its top and bottom (Supplementary Fig. S1C).

#### 2.1.1. Fabrication of the apical and basal PDMS layers

The apical and basal channel layers were made by first spin coating and curing a single (200 μm, basal channel) or multiple (1000 μm, apical channel) layers of PDMS elastomer (10:1, base:curing agent, Ellsworth Adhesives, Cat. no. 4019862) on PC substrate and curing for 2 h to overnight at 60 °C. The microfluidic features of the apical and basal channels were then made by cutting the designs of the main channels, vacuum chambers, and the inlet and outlet ports in the PDMS layers using a Graphtec (CE5000-60) Vinyl Cutter.

#### 2.1.2. PC layers with integrated TEER and oxygen sensors

In-house designed PC sheets with patterned gold electrodes and cut-out inlet and outlet ports (LasX Industries Inc.) were first cleaned with 100% isopropyl alcohol (IPA) and plasma treated on the surface (40 s of oxygen supply at 0.8 mbar and 20% power, Nano-plasma system, Diener electronics GmbH & Co. KG) followed by incubation in freshly made 5% (3-Aminopropyl) triethoxysilane (Sigma-Aldrich, Cat. no. 440140) in deionized water for 20 min. Similarly, the apical and basal PDMS parts were plasma treated and incubated in freshly made 1% (3-glycidyloxypropyl)trimethoxysilane (Sigma-Aldrich, Cat. no. 440167) in deionized water for 20 min. The silane treated parts were then thoroughly washed with deionized water to remove the excess chemicals, dried with compressed air, and immediately aligned and bonded with the corresponding apical or basal PDMS layers with the gold electrodes facing towards the apical and basal channels. The bonded parts were left at room temperature for 30–40 min to end the silane activation time before their overnight incubation at 60 °C under 0.5–1 kg weights.

Oxygen sensors were added to the PC walls of the apical and basal part by depositing small volumes (0.4–0.5 μl) of 10 mg/ml oxygen sensing nanoparticles (OXNANO, Pyroscience) in chloroform slurry at two different locations in each of the apical and basal channels, one location close to the inlet and one close to the outlet ports (Supplementary Fig. S1C).

#### 2.1.3. Fabrication of permeable PDMS membrane

The permeable PDMS membranes separating the apical and basal channels were fabricated in-house using an Automated Membrane Fabricator (AMF 9000) machine. The membrane was designed to be a thin (50 μm) PDMS layer consisting of an array of uniformly distributed pores (7 μm diameter, 40 μm spacing) that allows nutrients and small molecules to travel across the channels but not the mammalian cells. Silicon wafers (4 cm × 4 cm) patterned with an array of pillars (7 μm diameter, 50 μm height, 40 μm spacing) were used as a mold to shape the PDMS into the thin, porous membrane. To make these membranes, the wafers were placed in designated slots of the AFM 9000 tray, and PDMS elastomer mix (10:1 base:curing agent) was freshly made and poured onto the center of each membrane wafer post array (0.09 ml/wafer) and allowed to rest for at least 5 min to cover >75% of the posts. Square cut pieces (4.5 cm × 4.5 cm) of PC sheets treated with plasma were gently laid onto the PDMS on the plasma-treated side. Each assembly was then layered with a square shape spacer (1 cm PDMS block) on top of the PC sheet for making a uniform membrane thickness. The membranes were placed into the AFM 9000 machine to cure overnight following a

stepwise temperature increase from 20 to 60 °C at 40 Psi pressure.

#### 2.1.4. siChip assembly

To assemble the dual-channel siChip, the apical part and PDMS membrane were first treated with plasma on their exposed surfaces and gently bonded together followed by 2 h of incubation at 60 °C. The basal ports were opened using fine-tip forceps to give access to the basal channel. The apical and basal parts were then treated with plasma, carefully aligned, and bonded to make the complete dual-channel siChip (Supplementary Fig. S1C), which was incubated overnight at 60 °C under a uniform load of 1 kg weights arrays for full bonding.

#### 2.1.5. siChip assembly on a customized PCB

A customized PCB (cPCB, OSH Park, USA) was designed to fit the siChip within the board for direct access to the TEER sensors on-chip and to make a flushed 1.65 mm thick PCB layer that is seamlessly integrated with the Pod™ (Emulate Inc.). The siChip was mounted on the cPCB using the four pads connecting the TEER electrodes to the PCB circuit using silver epoxy conductive adhesive (AI TECHNOLOGY INC, Cat. no. EG8050) (Supplementary Fig. S1D) cured overnight at 80 °C. To seal-off the integration areas on the cPCB, the top and bottom surfaces of cPCB with incorporated siChip were covered and laminated with a thermal adhesive layer (3M Thermal Bonding Film 583) followed by attaching a 1 mm thick PDMS layer on top using thermal lamination at 120–140 °C (Supplementary Fig. S1E).

#### 2.1.6. pH sensor integration

pH sensor spots (PyroScience, PHSP5-PK5) were integrated into the effluent reservoirs of the commercially available Pod™. Frosted surfaces of the reservoirs were coated with a thin layer of silicone glue (SPGLUE, PyroScience GmbH) to maximize the surfaces optical clarity and signal transmission during measurements. The pH sensor spots were then glued to the inner walls of the Pod™ at the closest proximity to the outlets and allowed to dry overnight in the dark.

#### 2.1.7. Modified Pod™ fabrication and assembly

Using Fortus 400mc 3D Printer (ABS-M30 material, Stratasys, USA), we fabricated a base compartment for modified Pod (mPod) to connect the siChip-on-cPCB seamlessly to Pod™ reservoir. The base is constituted of detachable back and front parts with two openings in the back for accessing the cPCB and optical imaging of the culture on-chip, respectively (Supplementary Fig. S1F). The chip was assembled on mPod by first placing the siChip-on-cPCB on top of the 3D printed base followed by adding the Pod™ portable reservoir, closing the front insert of the base and then securing all the compartments together using 3 metal screws at the bottom of the base.

#### 2.1.8. Modified tray

A modified Tray (mTray) inspired by the commercial Zoë™ Culture Tray (Emulate, Inc.) was 3D printed and equipped with electrical connections to connect the pins from the Tray slots to a serial connector located at one end of the mTray for access from outside the incubator via a serial cable. All the components of the siChip, cPCB, mPod, and mTray were designed using SOLIDWORKS® (Solidworks Premium, 2020 SP4.0).

#### 2.1.9. Compartment sterilization

All in-house fabricated parts including the siChip, cPCB, and mPod were sterilized using plasma cleaning treatment at 4 s of oxygen supply, 0.3 mbar, and 100% power (Nano-plasma system, Diener electronics GmbH & Co. KG) before chip activation and cell seeding.

### 2.2. siChip activation, cell seeding, and culture

#### 2.2.1. siChip activation and extracellular matrix (ECM) coating

The sterilized siChip was desiccated for 30 min before 70% ethanol

was washed through the apical and basal channels followed by a one-time wash with tissue culture-grade water. The polymeric surfaces of the membrane were then chemically functionalized with 0.5 mg/ml ER1 in ER2 buffer (Emulate™ Inc., USA) under an ultraviolet lamp (Nailstar, NS-01-US) first for 10 min followed by additional 5 min after refreshing the ER1/ER2 buffer in the channels. Both apical and basal channels were then sequentially washed with ER2 buffer and cold Dulbecco's Phosphate-Buffered Saline (DPBS). For the Gut Chip, the PDMS membrane surfaces in the apical and basal channels were coated with 30 µg/ml Collagen I (Advanced BioMatrix, Cat. no. 5005) and 100 µg/ml Matrigel (BD Biosciences) in cold PBS. For the Liver Chip, following previously published protocols (Farooqi et al., 2021; Kulsharova et al., 2021; Menon et al., 2014), the apical channel surfaces were coated with 30 µg/ml fibronectin (Corning, Cat. no. 356008) and 400 µg/ml Collagen I (Advanced BioMatrix, Cat. no. 5005) in cold DPBS, while the basal channel was coated with 100 µg/ml Matrigel (BD Biosciences) and 200 µg/ml type I collagen in cold DPBS. The ECM loaded siChips were incubated for 1.5–2 h at 37 °C, followed by one time wash with warm respective culture medium in each channel. Culture medium for the 4 cell lines were vacuum filtered prior to use, to get rid of micro-air bubbles that could hamper the flow in the siChip.

#### 2.2.2. Cell seeding

To create the Gut Chip, primary human umbilical vascular endothelial cells (HUVECs; 6–8x10<sup>6</sup> cells/ml) were first seeded on the basal side of the PDMS membrane and then the chip was immediately inverted and incubated for 2–3 h at 37 °C to allow cell attachment on the basal side of the membrane. The chips were flipped again and the channels were perfused with warm culture medium both apically and basally before seeding human Caco-2 intestinal epithelial cells (Harvard Digestive Disease Center; 2–3x10<sup>6</sup> cells/ml) in the apical channel. The chips were then incubated overnight at 37 °C under static conditions to allow cell attachment. The next day the chips were perfused with endothelial growth medium (Lonza, EGM™-2 BulletKit™, Cat. no. CC-3162) in the basal channel and Caco-2 growth medium (15% FBS in DMEM) in the apical channel.

To create the Liver Chip, human liver endothelial cells (LECs) (Lonza HLECP1; 4–5x10<sup>6</sup> cells/ml) were first loaded in the basal channel followed by seeding of human Huh7 hepatocytes (Sekisui JCRB0403-P; 2.5–3.5 × 10<sup>6</sup> cells/ml) in the apical channel following the same method described above for the Gut Chip. After overnight incubation at 37 °C, the channels were perfused with the Huh7 growth media (10% FBS in DMED) apically and LECs growth media (Lonza, CC-3162) basally before starting the culture.

#### 2.2.3. Culture of siChips in the commercially available culture instrument

To culture the seeded siChips in the Zoë™ Culture Module (Emulate, Inc), the Pods™ were first primed with the endothelial and epithelial media in the basal and apical channels, respectively, to remove any air from the microfluidics that connect the reservoirs to the chip. The Pod™ reservoir with the attached microfluidic compartment was then removed from the commercial base, integrated with the siChip on the mPod, and placed in the mTray inside the Zoë™ Culture Module before starting the automated flow perfusion while placed in a 37°C incubator (Supplementary Fig. S2A). The Gut siChips were maintained under a continuous flow of Caco-2 growth medium apically and endothelial growth medium basally at 40 µl/h for 10 days before changing to differentiation-promoting media (5% FBS in DMED apically and 0.5% FBS basally) for the rest of the culture time. The Liver siChips were also maintained under a continuous flow of Huh7 growth medium apically and LECs growth media basally at 30 µl/h for 5–6 days before reducing the media FBS content for induction of tissue differentiation (5% FBS in DMEM, apically and 0.5% FBS, basally).

## 2.3. Continuous measurement of TEER, oxygen, and pH on-siChip

### 2.3.1. TEER measurement and analysis

TEER was measured continuously while siChips were in culture in the mTray inside the Zoë™ culture instrument. The mTray was connected to a CompactStat.h Mobile electrochemical interface (B32121, Ivium Technologies B. V., The Netherlands) outside the incubator using a serial cable. The TEER was measured following the method previously reported by Henry et al., (2017). Briefly, a four-point impedance measurement was taken periodically every 1–2 days using the IviumSoft application (V4.97, Informer Technologies, Inc.) paired with the CompactStat.h electrochemical interface. A current of 100  $\mu$ A was applied between the two excitation electrodes located on the opposite sides of the siChip membrane and the drop in the potential was measured in the second set of electrodes. For each chip, the impedance spectra were recorded over a range of frequencies varying from 10 Hz to 100 kHz. The impedance at high frequencies (>10 kHz) is mainly characterized by the media resistance while at lower frequencies (<100 Hz) the TEER from the tissue electrical resistance dominates the impedance signal (Henry et al., 2017). The TEER of the epithelial-endothelial tissue interface was obtained by subtracting the impedance at 100 kHz (system background impedance) from that at 100 Hz reported as the Organ Chip tissue impedance ( $\Omega$ ). The baseline impedance of empty chips perfused with DPBS was measured to ensure the negligible resistance of the membrane or correction for any background resistance. Throughout the culture, the impedance of siChip was continuously measured every 1–2 days and up to 23 and 12 days for Gut and Liver siChips, respectively.

### 2.3.2. Oxygen measurement and analysis

Oxygen measurements were performed using FireSting®-O<sub>2</sub> Optical Oxygen and Temperature Meter system (FSO2-C4, Pyroscience sensor technology, Germany) controlled using Pryo Oxygen Logger (V3.317©, Germany). To measure the oxygen levels, siChip was placed on a slide warmer (XH-2002, Premiere®) set at physiological temperature of 37 °C while the sensing optical fiber (Pyroscience, Cat. no. SPFIB-BARE) was placed perpendicular to the oxygen sensitive spot on-chip for maximum signal intensity (Supplementary Fig. S2B). The oxygen sensor spot was illuminated with red light (610–630 nm wavelength) and the luminescence emission was collected at near-infrared (NIR) (760–790 nm wavelength) for 10 consecutive seconds (one measurement per second). A fiber optic Pt100 Temperature Probe (Pyroscience, Cat. no. TDIP15) was also used for simultaneous temperature measurement on-chip. The measured signal intensity was converted to dissolved %O<sub>2</sub> using the Oxygen Calculation Tool (©2019 Pyroscience, Germany). We calibrated the FireSting® system with a 2-point calibration method using 100% and 0% dissolved oxygen calibration solutions following Pyroscience Sensor Technology (Germany) instructions. Briefly, oxygen-sensitive detection spots were immobilized at the flat bottom of two plasma-treated glass containers; one was half-filled with dH<sub>2</sub>O and thoroughly mixed several times to achieve 100% dissolved oxygen (%21 O<sub>2</sub>), and one filled with 0% O<sub>2</sub> deoxygenated solution made by mixing one OXCAL calibration capsule (Pyroscience) in 50 ml dH<sub>2</sub>O. For Gut and Liver siChip oxygen measurements, representative oxygen tension levels were obtained from the average of 10 consecutive measurements across all of the four sensor locations on-chip.

### 2.3.3. pH measurement and analysis

pH measurements were performed using the FireSting®-PRO Optical PH and Temperature Meter (FRPRO-4, Pyroscience sensor technology, Germany) controlled by Pyroscience Workbench software (V1.2.3.1406, Germany). Similar to oxygen sensing, pH was measured by placing the contactless fiber optic (Pyroscience, Cat. no. SPFIB-BARE) perpendicular to the pH sensor spot, illuminating the spots with the red light through the transparent wall of the reservoir pod and collecting the reflected NIR light over 10 s (Supplementary Fig. S2B). The measured signal intensity was converted to pH level using the calibration parameters in the Pryo

Workbench software. We calibrated the FireSting®-PRO Meter using a 2-point calibration method with pH 2 (PHCAL2, Pyroscience) and pH 10 (PHCAL10, Pyroscience) calibration solutions when pH sensors were mounted on the glass vials.

### 2.3.4. Automated imaging and analysis of metabolic cell activity on-siChip

Metabolic activity of the liver cells was measured continuously using Perceval reporter sensor (lentivirus particle pLV[Exp]-Puro-CMV:T2A:mCherry/3xNLS) (VectorBuilder.com) (Berg et al., 2009) transduced in the Huh-7 cells combined with an in-house developed automated fluorescent microscopy system compatible with the Zoë™ Culture Module. Perceval(ns) ORF and nuclei (mCherry/3xNLS ORF) reporters (Berg et al., 2009) respectively allow for live sensing of the ATP/ADP (adenosine-triphosphate to adenosine-diphosphate) concentration ratio and cell viability. The Perceval sensor offers high-affinity binding site to ATP molecules (prominent peak at 490 nm wavelength), but when the ATP levels decrease, ADP molecules (small peak at 405 nm wavelength) bind to the same site leading to a binding competition between the two substrates which induces a ratiometric change in the YFP/CFP excitation spectrum that provide a readout for the ATP/ADP ratio. The T2A:mCherry nuclear localization reporter is a live cell marker that uses a peptide produced by living cells that binds to proteins entering the nucleus, which release the fluorescent mCherry reporter. To continuously image the YFP/CFP/mCherry signal in the living chip cultures, we developed a customized microscopy module inside the incubator built on a XYZ translation stage (Zaber Corp) for providing micron positional accuracy along with a CFP/YFP/mCherry multiband filter set (Chroma) that also offers narrow LED excitation bands (405, 505, and 565 nm, Thorlabs). A dock was designed above the microscope to accommodate the Zoë™ with cut through openings that provide optical access to siChips while cultured inside the Zoë™. The microscopy platform was controlled using a Python-based graphical user interface (GUI) developed in-house that allows for the design of the experimental setup, as well as control of the three-axis linear stages, camera components, light settings, automated timelapse imaging, and autofocusing capabilities.

At each timepoint, fluorescent images of the living siChips were acquired automatically at 10 different locations along the length of the apical channel at the three wavelengths (RFP for nuclei and YFP and CFP for ATP/ADP ratio). An automated image processing pipeline was also developed using open-source CellProfiler (cellprofiler.org) software to automatically perform the following analysis on each acquired image: 1) identify nuclei with RFP marker, 2) define a cell as 4 pixels surrounding the edge of each nucleus, 3) measure YFP and CFP signal intensities and the YFP/CFP ratio in each cell, 4) count cell numbers per image, 5) track changes in YFP and CFP signal intensity over time, and 6) average the YFP/CFP ratio over all cells per image and normalize it to total cell count. ImageJ (Version 1.53) was used to divide the YFP and CFP signal intensities and obtain ATP/ADP images representing metabolic activity changes in the siChip.

## 2.4. Continuous measurement of metabolic functions in response to chemical stimulation and bacteria co-culture on siChip

The baseline levels of TEER, oxygen, pH, and ATP/ADP ratio in siChips were measured up to two days before starting the treatments to ensure the stability of the metabolic activities before any external stimuli were added.

### 2.4.1. Calcium chelation treatment to disrupt cell-cell junctions

Ethylene glycol-bis(2-aminoethyl ether)-N, N, N', N'-tetraacetic acid (EGTA) is a high affinity calcium chelator that can reversibly disrupt epithelial tight junctions by reducing free calcium concentration in the culture medium (Rothen-Rutishauser et al., 2002; Samak et al., 2011). Gut and Liver siChips were treated at day 14 and 6 of culture, respectively, with 5 mM EGTA (Sigma, Cat. no. E3889) in dH<sub>2</sub>O that was added to the media of both apical and basal channels and perfused

continuously for 30–45 min before starting the measurements. The TEER was measured continuously every 20–30 min and oxygen was measured every 30 min to 1 h throughout the 2.5–3 h of the treatment. After 3 h, the chip media was replaced in both channels with fresh (no EGTA) culture media and the culture was continued for recovery overnight. The impedance and oxygen levels were measured at multiple time points during recovery until normal metabolic functions were resumed on-chip. Bright field and immunofluorescence microscopy imaging was also performed non-invasively throughout the EGTA treatment and recovery time.

#### 2.4.2. Oligomycin (OM) treatment

Gut and Liver siChips were treated, at day 17 and 12 of culture, respectively, with 1  $\mu\text{M}$  oligomycin A (Sigma-Aldrich, Cat. no. 75351) in the epithelial and endothelial media perfused continuously in the chip for 3 h before starting the measurements. Control siChips were treated with media containing 0.5% DMSO (OM drug carrier). After 24 and 5 h of treatment in Gut and liver siChips, respectively, the media was changed to fresh (non-OM) media to start the tissue recovery. The impedance and oxygen levels were measured continuously during treatment and up to 3 days during the recovery. Bright field and immunofluorescence (nuclear reporter, ATP/ADP ratio in Huh-7 cells) microscopy imaging was also performed before and during the treatment as well as after the recovery.

#### 2.4.3. *Lactococcus lactis* (*L. lactis*) bacteria co-culture

*Lactococcus lactis* subsp. *cremoris* MG1363 (*L. lactis*) (ATCC, Cat. no. 19257) was inoculated in the apical epithelium channel of the Gut Chip on day 13 of culture. To remove any antibiotic or buffering capacity from the media, the chips were perfused with a customized low buffer Hanks Buffer Salt Solution (HBSS, pH 5.1) in the apical channel and with antibiotic-free media in the basal channel 24 h prior to bacterial inoculation. The customized HBSS solution allows modulation of the pH during the co-culture time. The chips were inoculated with *L. lactis* ( $10^3$  CFU/ml) at 37 °C for 1–2 h under static conditions before resuming continuous flow on the chip in the Zoë™ Culture Module. *L. lactis* co-culture on Gut Chip was maintained for 4 days and the pH level of the apical and basal endothelium channels were continuously measured every 24 h.

#### 2.4.4. Immunofluorescence staining and imaging

At the endpoint of experiments, siChips were removed from the mPods, washed two times with DPBS, fixed with 4% paraformaldehyde for 15–20 min at room temperature, and incubated overnight in 1:100 anti-H2AX antibody (Novus Bio NB100-2280) at 4 °C in 1% BSA in PBS and 0.01% Triton-X 100. The chips were washed with PBS containing 0.01% Triton-X 100 twice before incubation in the secondary antibody (1:1000 anti-rabbit 555) and 1:10,000 DAPI, and imaging on a Zeiss LSM 710 with a 32 $\times$  water objective.

### 2.5. Statistical analysis

All results are presented from at least two independent experiments and data points are shown as mean  $\pm$  standard error of the mean (s.e.m.) from multiple chips. Statistical analysis was performed using GraphPad Prism version 8.0 (GraphPad Software Inc., San Diego, CA) and the statistical significances between groups were tested using two-tailed Student's *t*-test, unpaired multiple *t*-test or One-way ANOVA with Tukey correction for multiple hypothesis testing.

## 3. Results and discussion

### 3.1. Fabrication of the siChips with TEER, oxygen, and pH sensing capabilities

The siChip was designed to enable three main capabilities: i)

recapitulation of the tissue physiological structure and microenvironment, ii) non-invasive and continuous sensing of multiple metabolic functions, and iii) compatibility with a commercially available tissue culture module for automated and multiplexed Organ Chip culture. The siChip including both the porous membrane and layers containing the apical and basal channels was fabricated from flexible PDMS polymer and integrated using a layer-by-layer assembly approach to allow implementation of biomechanical stimulation (e.g., peristalsis-like motions). Flat sheets of rigid PC material containing integrated TEER electrodes and oxygen sensors and cut to the same size and shape as the chip were bonded to the top and bottom surfaces of the chip to minimize gas permeability and measure epithelial barrier function and oxygen levels, respectively (Fig. 1A). The sensors detect free oxygen molecules in the pericellular microenvironment of the tissue and were placed at four different locations in the siChip (two in apical and two in basal channels) to fairly represent tissue oxygen levels across the whole chip. These sensing spots are easily and non-invasively accessible through the optically clear PC layer on the top and bottom sides of the siChip allowing continuous, real-time oxygen measurements in living chip cultures throughout the entire experiment (Fig. 1B, Supplementary Fig. S1C).

The integrated TEER sensors also enabled remote and continuous monitoring of tissue barrier function on-chip. A customized PCB (cPCB) with compatible configuration to the commercial organ chip holder (Pod™, Emulate Inc.) was developed for both direct access to the TEER electrodes and seamless integration of the siChip into the Pod™ (Fig. 1B). This was facilitated by 3D printing a base compartment to create a modified Pod™ (mPod) (Fig. 1C, Supplementary Fig. S1F). To measure pH levels on-chip, we integrated pH sensors in close vicinity of the apical (epithelial) and basal (endothelial) channel outlets. The mPCB and mPod designs enabled seamless integration of the siChip within the commercially available, automated Zoë™ Organ Chip culture module. The design also allowed for non-invasive access to all the integrated sensors (e.g., TEER, oxygen, pH) through an opening in the mPod that overlaid the chip channels permitting continuous measurements, frequent optical imaging, and metabolic monitoring of live chip cultures (Fig. 1D, Supplementary Figs. S2A and B). We also developed a modified Tray (mTray) that provides direct and simultaneous access to the mPCB of 6 siChips in parallel and hence, remote measurement of TEER while the siChips are cultured in the Zoë™ culture instrument. Each mTray consisted of an array of built-in spring-loaded electrical contacts in the base of each slot for direct contact with the cPCB in each siChip. Using a serial connector, the electrical signals sensed from all siChips are transferred out via a serial cable enabling remote data collection from outside the incubator (Fig. 1E, Supplementary Fig. S2A). We used a combination of in-house customized designs and fabrication techniques with a commercially available system to simultaneously maximize the non-invasive and functional sensing capabilities, user-friendly operation of the device, and enhance manufacturing potential, biocompatibility and clinical relevance.

To ensure that the integrated oxygen and pH sensors provided accurate, reproducible, and long-term stable measurements of tissue metabolic activity, the siChips were perfused with solutions of known oxygen or pH levels using the Zoë™ Culture Module operated inside the incubator (37 °C, 5%CO<sub>2</sub>) for 3–14 days while measuring oxygen and pH levels. Continuous perfusion of 0% and 100% (21% O<sub>2</sub>) air saturated solutions in the siChips and on-chip measurements confirmed the accuracy and stability of the oxygen tension signals as well as the sensors' signal consistency in the apical and basal channels (Fig. 1F). The long-term stability and accuracy of the pH sensors under tissue culture conditions over time were also confirmed using pH 2 and 5.5 solutions perfused through the siChips for 14 days. Results obtained using the on-chip pH sensors and in standard calibration glass containers were comparable. Additionally, oxygen plasma treatment (used for siChip sterilization before cell culture) did not affect the sensor's functionality (Fig. 1G). These results collectively indicate that the bespoke siChip and

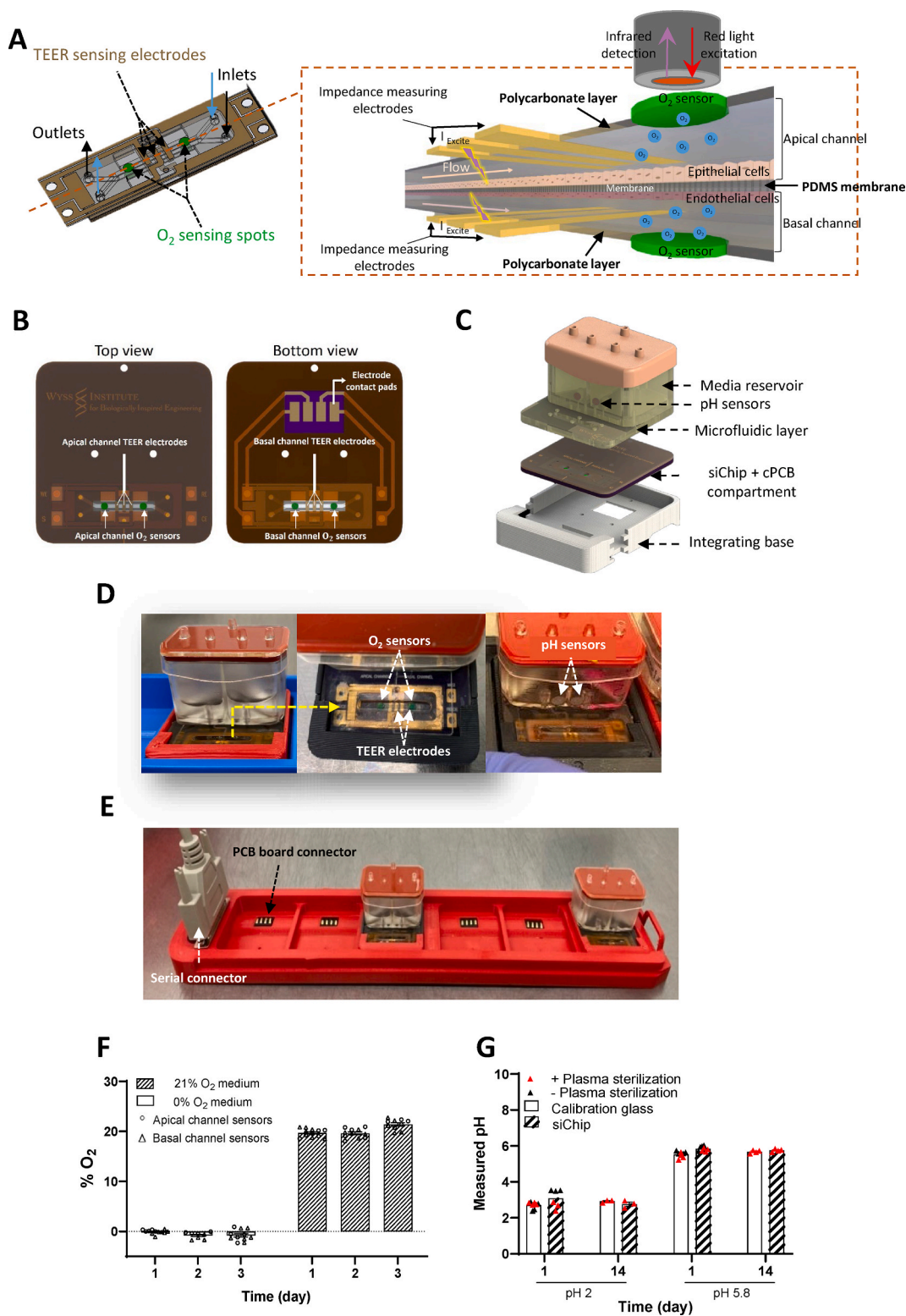


**Fig. 1. Design, fabrication, and validation of measurements in sensor integrated Organ Chip (siChip).** A. Schematic view of the dual channel chip with integrated TEER and oxygen sensors (left) and magnified cross section view of the chip (right). B. Schematic of the top and bottom views of the assembled siChip on customized PCB (cPCB). C. Assembly of the siChip on cPCB with Pod™ media reservoir to make a modified pod (mPod). D. Photographs of the final siChip device with integrated TEER, oxygen, and pH sensors for automatic flow perfusion and culture in Zoe™ Culture Module. E. Photograph of the modified Tray (mTray) with pin connectors for continuous and remote TEER measurements. F. Validation of oxygen sensors measurements in siChip with 0% and 21% O<sub>2</sub> calibrating solutions. G. Validation of pH sensors measurement before and after siChip sterilization as compared to standard calibration glass using pH 2 and pH 5.8 solutions. n = 6 (F) and 4 (G) individual siChips per group.

integrated analytical sensors maintain their integrity, function, and measurement accuracy during long time experiments under physiologically relevant tissue culture conditions.

### 3.2. Non-invasive monitoring of metabolic functions in Gut and Liver siChips

We validated the biocompatibility and functionality of the integrated sensors by creating Gut and Liver Chips using the siChip devices and monitoring tissue viability and metabolic activity. In the Gut siChip, human Caco-2 intestinal epithelial cells and human umbilical vein endothelial cells (HUVECs) were cultured on the apical and basal surfaces of the ECM-coated membrane, respectively, to create a physiologically relevant epithelial-endothelial tissue interface, which recapitulates many features of the human small intestine, including intestinal villi formation, drug metabolizing activity, and mucus production, as described previously (Jalili-Firoozinezhad et al., 2019; Kim et al., 2012). As observed in past Gut Chip studies, the epithelial cells formed a uniform monolayer at day 1, developed into a dense villus epithelium by day 10, and accumulated a thick mucus layer by day 23

that obscured the epithelium below (Supplementary Fig. S3A).

A Liver siChip was similarly developed by seeding Huh7 liver epithelial cells that are well characterized (Kawamoto et al., 2020) and liver sinusoidal endothelial cells (LSECs) on the apical and basal sides of the chip porous membrane, respectively. Phase contrast images of the chips showed formation of a uniform cell monolayer at day 1 that formed a dense tissue by day 4, 8, and 12 on siChip (Supplementary Fig. S3B), similar to previously reported established Liver Chip that used Huh7, HepG2 or hiPSC-derived hepatocytes (Farooqi et al., 2021; Kulsharova et al., 2021; Lee-Montiel et al., 2020; Menon et al., 2014).

#### 3.2.1. Continuous measurement of barrier function on siChips

Barrier function plays an important role in epithelial tissues in health and disease and thus, we used our integrated TEER electrodes as a label-free, noninvasive way to analyze barrier properties (impedance) of the Gut and Liver siChips every 1–2 days over more than 3 weeks in culture while under continuous flow on-chip. In the Gut siChips, we detected an electrically resistant intestinal barrier with an impedance of  $>2,000 \Omega$  at day 1 of culture, which remained relatively constant while the chips were perfused with the growth medium during the first 10 days of

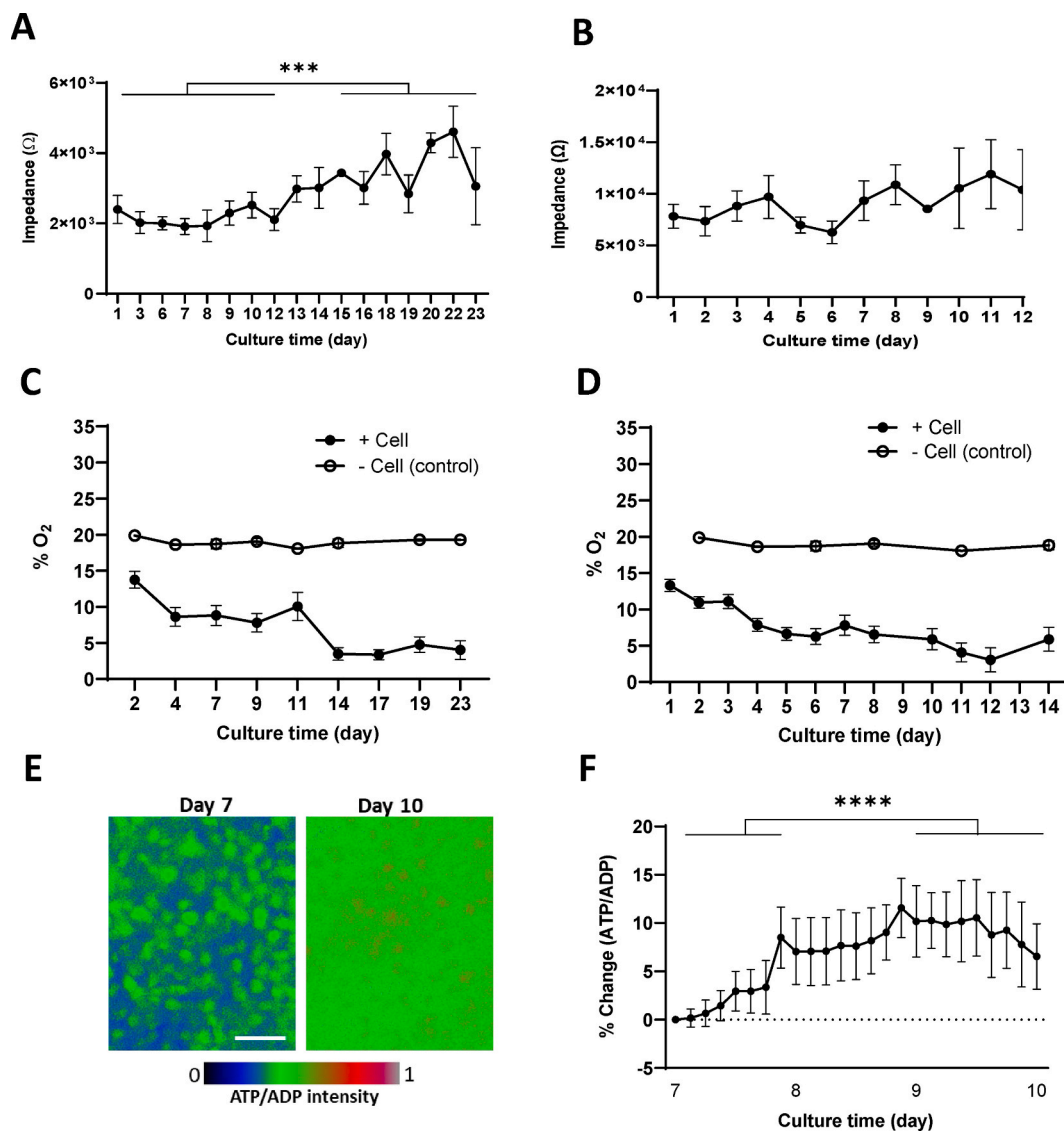


**Fig. 2. Non-invasive monitoring of metabolic functions in Gut and Liver siChips.** Continuous measurement of A, B, impedance, and C, D, oxygen tension in Gut (A, C) and Liver (B, D) siChips throughout the culture time. E. Fluorescence ATP/ADP signal microscopic images at day 7 and 10 of culture in Liver siChip. Scale bar 100  $\mu\text{m}$ . F. Continuous measurement of percentage change in ATP/ADP fluorescence signal in Liver siChip over 3 days of culture. Data represent the mean  $\pm$  s.e.m.; n = 4–9 (A), 5–9 (B), 5–13 (C), 15–25 (D), and 5 (F) experimental chip replicate.  $***P < 0.001$ ,  $****P < 0.0001$ .

culture; however, the impedance gradually increased (up to >1.5 fold) when the serum level was dropped in the perfused medium to induce cell differentiation (Fig. 2A). The higher levels of electrical impedance during the differentiation period compared to expansion period are consistent with past studies that showed an increase in epithelial tight junctions during the differentiation process (Varadarajan et al., 2019).

The continuous measurement of TEER in Liver siChip similarly showed the establishment of an electrically resistance (>7,800 $\Omega$ ) tissue barrier at day 1 of culture which increased up to >1.2 fold by day 4 and remained relatively stable during the rest of the 12 day experiment when a dense liver epithelium was established on-chip (Fig. 2B, Supplementary Fig. S3B).

Electrical impedance encompasses both resistive and capacitive properties of the tissue barrier. At a frequency range of 100 Hz to 10 kHz, the current cannot pass through the tissue layer and the measured impedance reflects the combined effect of cell-cell junctions in the epithelium and endothelium as well as the stored current in the cells, which represents the tissues' electrical capacitance (Morgan et al., 2019; Srinivasan et al., 2015). At the 100 Hz frequency used in this study, the measured impedance represents the tissue electrical resistance (Henry et al., 2017).

### 3.2.2. Continuous measurement of oxygen levels and ATP/ADP activity on siChips

Respiration is one of the key indicators of the cell and tissue metabolic activity and quantification of dissolved oxygen levels in culture medium can improve our understanding of tissue cellular functions in normal and disease states (Johannsen and Ravussin, 2009; McClelland, 2011). In addition, having a continuous measure of oxygen levels would enhance consistency and reproducibility in culture studies (Al-Ani et al., 2018). We leveraged the oxygen sensors that we integrated into the siChips (Fig. 1A) to measure the dissolved oxygen levels in the medium flowing through the epithelial channels of the Gut and Liver siChips every 1–3 days throughout the culture to monitor the epithelial cell respiration activity. In the Gut siChips, continuous oxygen measurements under culture conditions revealed that the oxygen level drops to <15% at day 2 and <10% at day 4 of culture based on cellular utilization of oxygen (Grant et al., 2022), after which it remains stable until day 11 corresponding to the end of the expansion period in culture. Changing the expansion medium to the low serum differentiation medium further reduced the oxygen tension to microaerophilic levels (<5%) by day 14, and this remained stable for the rest of the culture time (Fig. 2C). This finding is consistent with a higher rate of aerobic respiration (>80% drop in oxygen tension) in the dense and differentiated epithelium compared to proliferating epithelial cells (Supplementary Fig. S3C).

Continuous measurements of oxygen level in the Liver siChip revealed that the tissue reduces the oxygen levels in the medium to <15% as early as day 1 in the culture, and this continues to drop reaching <5% by the end of the cell expansion period at day 5. As the Liver siChip continues to grow during the differentiation time, the oxygen level stabilizes at ~5–7% with >80% drop in oxygen level compared to day 1 (Fig. 2D, Supplementary Fig. S3D).

We also continuously measured the metabolic activity and viability of the epithelial cells expressing reporters for ATP/ADP and T2A: mcherry NLS (nuclear localization signal) in the Liver siChips by measuring the fluorescent intensity of the ATP/ADP ratio and cell nuclear signals, respectively. Continuous fluorescent imaging of siChips every 30–60 min showed an increase in the ATP/ADP ratio at day 10 compared to day 7 of culture and revealed a 6.5% increase in liver cell metabolic activity over 3 days of culture during differentiation (Fig. 2E, F). Continuous monitoring of the RFP nuclei signals also showed that the Huh7 cells remain viable on-siChips throughout the 12 days of culture (Supplementary Fig. S3E). The Huh7 liver epithelial cell line was originally isolated from a liver carcinoma and it is known to have low enzyme and metabolic activity compared to primary human hepatocytes (Bulutoglu et al., 2020), but it can become more metabolically active as

it can continue growing past confluence over long periods of culture (up to 4 week) (Sivertsson et al., 2010). Transfecting the cells with fluorescent reporters provided additional continuous monitoring capabilities in the siChips that enabled both direct and quantitative measurement of cell metabolic activity and viability, as well as automated image focusing and acquisition that excludes dead cells from analysis.

In the body, intestine and liver organs maintain physiological homeostasis under microaerophilic oxygen tension; 0.4–10% O<sub>2</sub> in the intestinal lumen (He et al., 1999) and 5–8% in the liver (Carreau et al., 2011; Guo et al., 2017; Trepiana et al., 2017). Recapitulating similar microaerophilic oxygen tension in the Organ Chips has been challenging in chips made of PDMS (Jalili-Firoozinezhad et al., 2019; Shin et al., 2019) due to the constant diffusion of the ambient air into the tissue channels that dominates any micro-modulation of the oxygen level by the cell's aerobic respiration. Here, we used thermoplastic PC polymer with limited oxygen permeability (Byrne et al., 2014; Mehta et al., 2009) in the top and bottom walls of the siChip to create a semi-isolated microenvironment for cells to physiologically modulate the oxygen levels to microaerophilic levels on-chip through aerobic respiration similar to that *in vivo* (Guo et al., 2017; He et al., 1999). This design further allowed us to model the effect of temperature on aerobic respiration in the intestinal epithelium, which revealed a higher oxygen consumption rate (up to 73%) in the Gut siChip at physiological temperature (37 °C) compared to room temperature (25 °C) (Supplementary Fig. S3F). The oxygen uptake in the ileus has been similarly reported to correlate with the lumen temperature consistent with the change in the metabolic rate (Kvietys et al., 1985). A temperature drop from 32 to 22 °C was reported to reduce oxygen consumption in the kidney and intestinal tissue by 75% (Hendriks et al., 2019; Kvietys et al., 1985), which is also similar to our observation in the Gut siChip further confirming the robustness of our system for modeling and sensitively monitoring tissue physiological responses to microenvironmental changes. The less permeable PC walls of the siChip also prevent absorption and adsorption of small, hydrophobic molecules (i.e. hormones and drugs) to the chip's bulk material (Auner et al., 2019), which can be a challenge in using PDMS chips, particularly in studies with highly lipophilic chemicals or drugs (Toepke and Beebe, 2006). Using flexible PDMS material in the main body of the siChip still allows for the application of cyclic biomechanical forces (i.e. peristalsis) when essential for tissue differentiation (Huh et al., 2010; Kim et al., 2012), which is an advantage compared to fully thermoplastic devices that cannot accommodate this functionality (Azizgolshani et al., 2021; Bussoo et al., 2022). Overall, our siChip design eliminates current technical challenges in creating physiological oxygen levels on-chip including anoxic medium perfusion in the channels or chip isolation inside an anaerobic chamber (Jalili-Firoozinezhad et al., 2019; Shin et al., 2019), while providing a confined microenvironment for cells to naturally establish relevant tissue/organ physioxia *in vitro*. These advancements expand the use of Organ Chip *in vitro* models in diverse and potentially higher throughput preclinical studies.

### 3.3. Continuous monitoring of responses to chemical and bacterial stimuli

#### 3.3.1. Dynamic monitoring of Gut siChip responses to environmental stimuli

To evaluate the sensitivity of the siChip system for continuous monitoring of functional and metabolic changes in the Organ Chips, we treated Gut siChips with chemicals and/or bacteria that are known to modulate epithelial tissue barrier, cell respiration, and pH. We exposed the Gut siChips to 5 mM EGTA for 3 h at day 17 of culture when the intestinal tissue had attained phenotypic and metabolic functional stability, and continuously measured TEER and oxygen levels during the treatment period and for up to 24 h after the EGTA was removed from the medium. Continuous on-chip TEER measurements showed >80% decrease in the impedance (from >2,000 $\Omega$  to < 800 $\Omega$ ) within 2 h after exposure to EGTA, which recovered to the pre-treatment level

(>2,400 $\Omega$ ) that also was similar to that measured in control Gut siChips within 12 h after removing the EGTA (Fig. 3A). Phase contrast microscopic imaging of the siChips revealed disruption of the opaque mucosal layer and retraction of the epithelium resulting in the appearance of large, rounded structures 3 h after exposure to the EGTA. Normal epithelial tissue morphology was fully recovered by 4 days after the EGTA was removed (Supplementary Fig. S4A).

Calcium chelating agents are known to modulate mitochondrial respiration in cells (Masola and Evered, 1984). Simultaneous measurement of oxygen levels on-chip revealed no change in the tissue respiration rate during the first hour of the treatment despite significant reduction (>70%) in the barrier function. However, after 3 h, oxygen levels had significantly increased up to 40%, representing a significant drop in the tissue aerobic respiration that reversed back to control, non-treated chip levels 17 h after removing the EGTA (Fig. 3B). The observed effect of EGTA on intestinal epithelial barrier resistance is also similar to that reported in previous studies (Azizgolshani et al., 2021; Henry et al., 2017). However, the multiplexing of the integrated TEER and oxygen sensors revealed simultaneous dynamic effects of EGTA on both barrier function and aerobic respiration in the intestinal tissue *in vitro*, which has not been reported before.

Oligomycin (OM) is a well-characterized antibiotic that binds to subunit of the mitochondrial ATP synthase and can significantly affect mitochondrial-dependent ATP production and cell respiration (Hao et al., 2010; Lee and O'Brien, 2010; Ruas et al., 2016). At day 17 of culture, OM (1  $\mu$ M) was perfused through the Gut siChip for 22 h and then removed while carrying out continuous on-chip monitoring of oxygen levels and TEER. Continuous oxygen measurements showed a significant (10-fold) increase in oxygen level after 22 h of treatment with OM, which further increased to >12-fold even after the OM was removed from medium, suggesting that some of the damage to epithelial cell respiration function was non-reversible (Fig. 3C). Continuous TEER measurements also demonstrated an adverse effect of OM on barrier function as indicated by a 25%–60% decrease in barrier impedance during exposure to OM that did not return to normal levels after termination of the OM treatment (Fig. 3C). Immunofluorescent microscopic imaging of the chip 22 h after treatment and 24 h after the recovery, respectively, showed an increase in the number of H2AX positive cells (>18%), indicating the presence of significant DNA damage in the chip epithelium, compared to untreated control chips (Fig. 3D). These adverse effects in DNA damage and oxygen respiration observed on-chip are consistent with previous studies that reported the detrimental effects of OM exposure in Caco-2 intestinal epithelial cells and HUVEC (JanssenDuijghuijsen et al., 2017; Patella et al., 2015).

pH homeostasis is also highly relevant for human tissue and organ physiology, as well as host interactions with bacterial and viral microorganisms (Espinosa, 2002; Hackett et al., 2016; Perdikis et al., 1998). Changes in pH have been observed in different diseases (Aoi and Marunaka, 2014; Lykke et al., 2021; Nakano et al., 2015) and thus, continuous quantitative measurement of pH *in vitro* can be a powerful tool to better understand dynamic tissue responses to different stimuli and insults. Because microbial interactions with host epithelium contribute significantly to control of tissue pH under both physiological and pathophysiological conditions (Jalili-Firoozinezhad et al., 2019; Perdikis et al., 1998; Plesniarski et al., 2021), we used our Gut siChip to continuously monitor pH levels when populated with living bacteria. On culture day 17, the chip was inoculated with *Lactococcus lactis* (*L. lactis*), a non-pathogenic, gram-positive bacterium that uses lactose or pyruvate for ATP formation and subsequent lactic acid production, which is known to dramatically decrease pH in the tissue microenvironment (Hugenholtz et al., 1993). Continuous pH measurements on-chip indicated that co-culture with the bacteria for 1–2 days resulted in a significant reduction in medium pH (from 7.2 to 4.5) in effluents of the epithelial channel, while the pH of the control chips without bacteria was maintained at a constant level ( $\sim$ pH 7) (Fig. 3E). In contrast, the medium pH of the endothelial effluents remained unchanged during this

same period, indicating that intestinal tissue barrier that prevented bacteria from entering the endothelium lumen remained intact. After 2 days, the pH of the endothelial medium dropped significantly to < pH 5, which is consistent with disruption of the tissue barrier resulting in invasion of *L. lactis* bacteria into the underlying endothelium. This was associated with a change in the color of phenol red containing endothelium medium from red ( $\sim$  pH 7.4) to yellow (acidic pH) with observable cloudiness representing overgrowth of bacteria in the medium (Supplementary Fig. S4B). Interestingly, the pH drop in the endothelial channel at these later times was accompanied by a simultaneous increase in the pH of the epithelium lumen (Fig. 3E). This may partially be explained by the overgrowth of bacteria in the epithelial channel resulting in a major depletion of nutrients and epithelial cell death and detachment at later times, which is consistent with results of immunofluorescence microscopic imaging of the epithelial layer (Fig. 3F). Once the barrier disrupted, the bacteria may move to the endothelial channel where higher nutrient concentrations are present leading to reduced numbers of lactic acid producing bacteria in the epithelial channel, and hence increased pH.

### 3.3.2. Dynamic monitoring of Liver siChip responses to environmental stimuli

Similar to the Gut siChip, we exposed differentiated Liver siChips to EGTA (5 mM) for 3 h and continuously monitored oxygen tension and barrier impedance on-chip throughout the treatment and recovery periods. Oxygen levels in the Liver siChip significantly increased and reached up to 80% higher values than before the treatment within 3 h of exposure indicating that aerobic respiration progressively decreased in the liver tissue with EGTA treatment, similar to what we observed in the Gut siChip. Moreover, removal of the EGTA restored normal tissue respiration and reduced the oxygen level back to control levels within 21 h (Fig. 4A).

Interestingly, continuous impedance measurements revealed an unexpected increase in barrier resistance (up to 6-fold) 1 h after the EGTA exposure that remained stable throughout the 2.5 h of the treatment and gradually dropped back to levels comparable to control chips after removing the EGTA at 24 and 72 h (Fig. 4B). This was accompanied by a greater than 1.5-fold increase in Huh7 epithelial cell size (projected area) compared to control untreated chips, as detected by live cell imaging (Fig. 4C and Supplementary Fig. S4C). The effects on TEER may be in part explained by an increase in cell proliferation as well as a decrease in cell motility mediated through store-operated calcium entry (SOCE) (Selli et al., 2015), which also has been shown to correlate with higher TEER levels in Huh7 cells (Morgan et al., 2019; Yang et al., 2013). SOCE is a cellular process activated by the depletion of calcium in the endoplasmic reticulum, triggering the opening of calcium channels in the plasma membrane and allowing calcium influx into the cell. Increased cell spreading enhances growth of many cells (Chen et al., 1997), including Huh 7 cells, while the opposite is true for migratory Huh7 cells (Berger et al., 2015). SOCE inhibition also has been associated with lower mitochondrial respiration (González-Sánchez et al., 2017), which is also consistent with the higher oxygen tension we observed during EGTA treatment in the Liver siChip (Fig. 4A). Additionally, we lowered the serum concentration of the medium 2 days before exposure to EGTA to induce tissue differentiation. The proliferative capacity of Huh7 cells in the presence of EGTA has been previously shown to be higher when they were pre-conditioned with serum-starvation compared to medium with high serum (Modica et al., 2019).

Similar to the Gut siChip, when we treated the Liver siChip with OM, we observed an increase in the number of DNA-damaged cells after 6 h and greater DNA damage 3 days after OM removal compared to control chips treated with the diluent (0.5% DMSO) alone (Fig. 4D). We also detected a significant (5-fold) increase in oxygen levels within 5 h after OM addition, which increased up to 10-fold even after OM removal, again indicating a reduced aerobic respiration capacity that was irreversible. OM treatment was also associated with a decrease in barrier

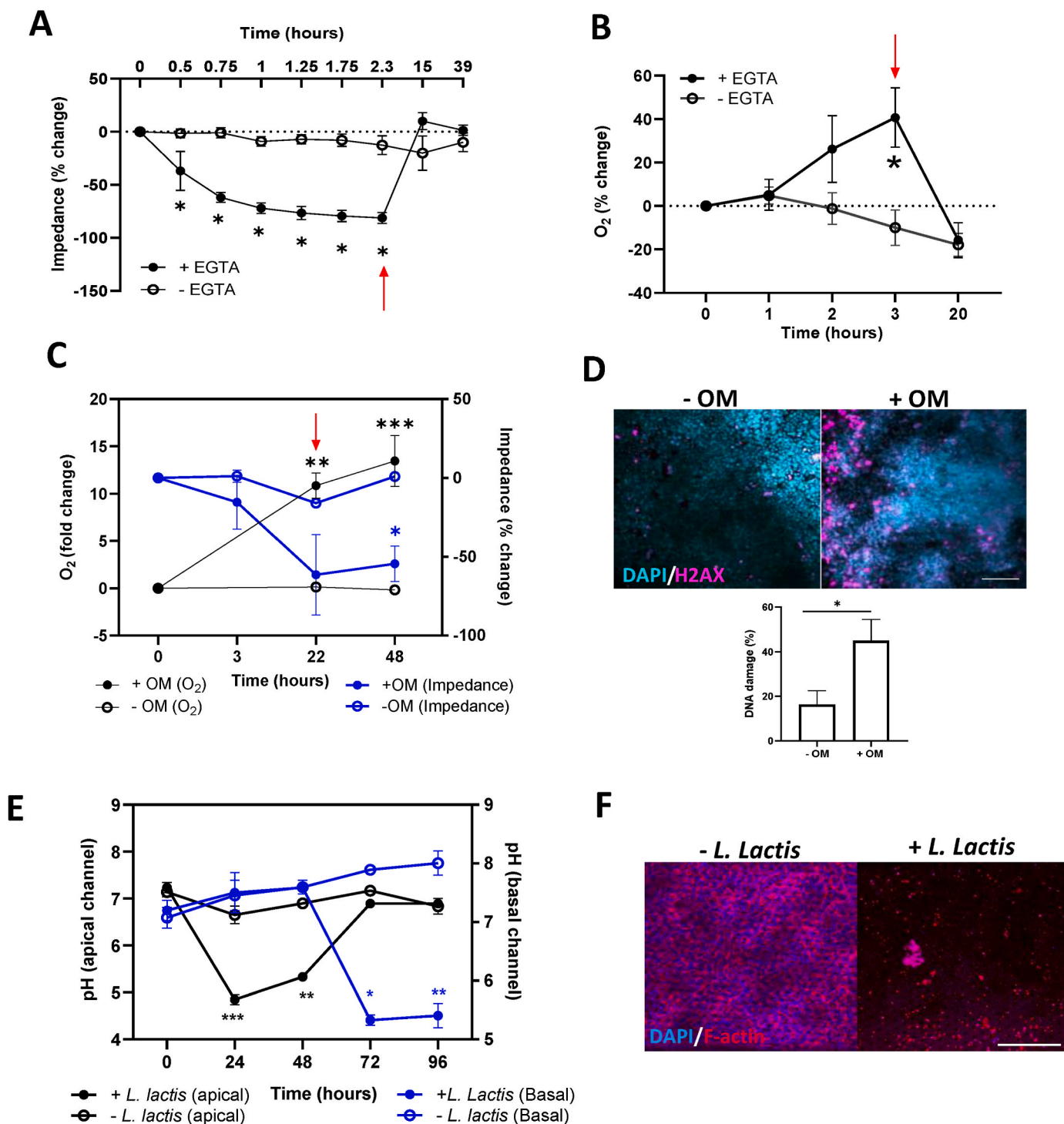


**Fig. 3.** Continuous monitoring of Gut siChip functional and metabolic responses to chemical and bacterial stimuli. **A.** Percentage change of impedance in Gut siChip with time during EGTA treatment and after it was removed. **B.** Continuous measurement of percentage change in oxygen level during EGTA treatment and post recovery. **C.** Change in the Gut siChip oxygen level (black line) and impedance (blue line) in response to oligomycin (+OM, closed circles) or its vehicle (-OM, open circles) exposure and after they were removed. **D.** Immunofluorescence images (top) of Gut siChip epithelium 48 h after treatment with OM compared to drug carrier stained with DAPI (nuclei, blue) and H2AX (DNA damage, magenta). Image-based quantitative analysis of percentage change in epithelial cells DNA damage with vehicle and OM treatment (bottom). Scale bar 100  $\mu\text{m}$ . **E.** Measurements of pH changes in outflows of epithelium (black line) and endothelium (blue line) lumens in response to *Lactococcus Lactis* (*L. lactis*) bacteria co-culture (closed circles) compared to no bacteria (open circles). **F.** Immunofluorescent microscopy images of the gut epithelium stained with DAPI (nuclei, blue) and F-actin (magenta) markers 96 h after inoculation with *L. lactis* bacteria. Scale bar 100  $\mu\text{m}$ . Data represent the mean  $\pm$  s.e.m.; n = 5 (A), 3 (B), 3–6 (C), and 3–6 (E) experimental chip replicate. \* $P < 0.05$ , \*\* $P < 0.01$ , \*\*\* $P < 0.001$ . Presented percentage and fold change values are normalized to pre-treatment levels. Red arrows indicate the end of EGTA or OM treatment in A,B, and C.

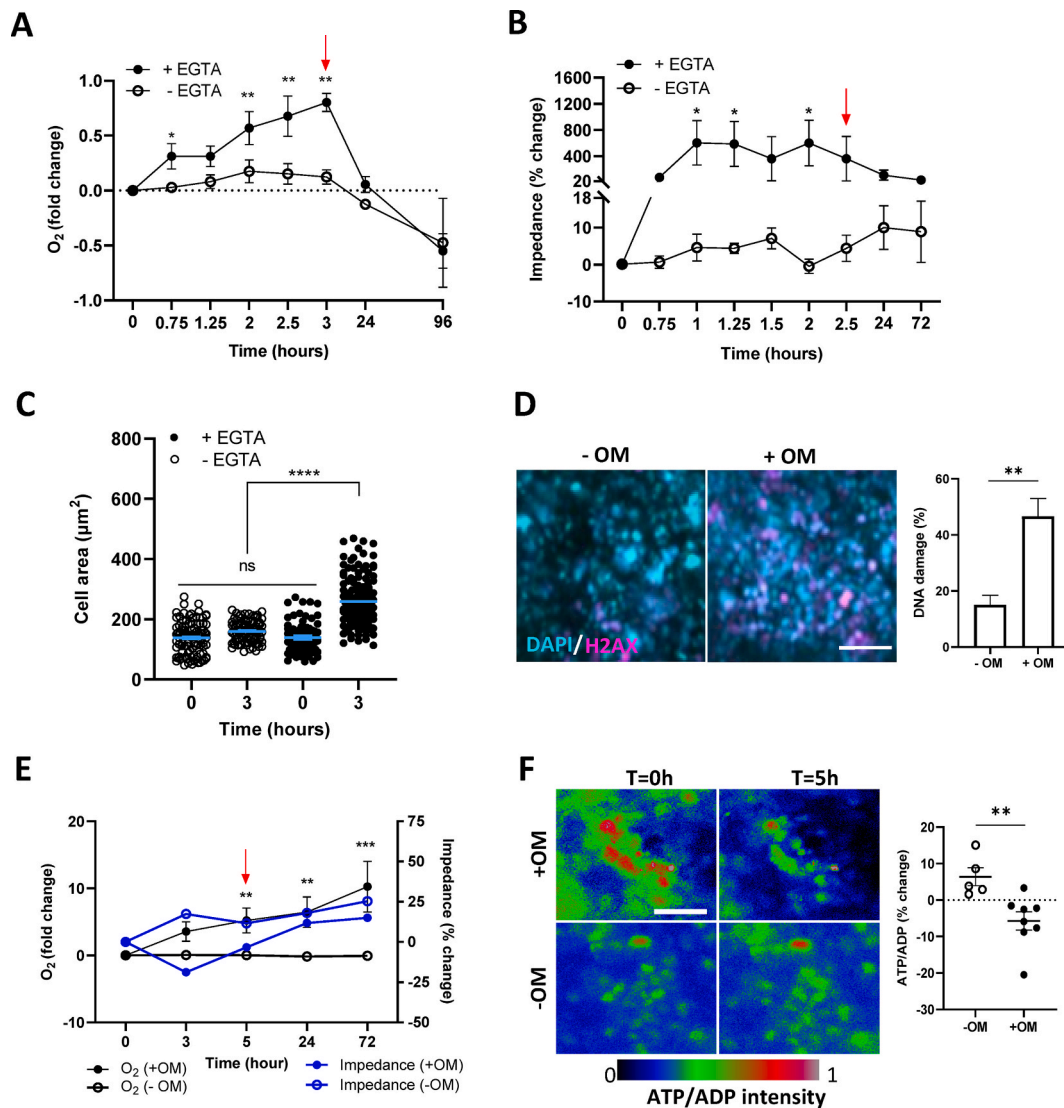


**Fig. 4. Continuous monitoring of Liver siChip responses to chemical stimuli.** Dynamic fold change in oxygen level (A) and percentage change in impedance (B) of Liver siChip throughout exposure to EGTA and after its removal. C. Quantitative analysis of epithelial cell size before and after 3 h of EGTA treatment compared to control chips with no EGTA. D. Immunofluorescent microscopic images (left) and quantitative analysis (right) of the DNA damage (H2AX<sup>+</sup> cells, magenta) in epithelium after exposure to OM compared to drug carrier. Nuclei stained with DAPI (blue). Scale bar 100  $\mu\text{m}$ . E. Dynamic changes in oxygen level (black line) and barrier impedance (blue line) after OM treatment (+OM, closed circles) and its removal compared to drug vehicle (-OM, open circles) treated siChips. Presented percentage and fold change values are normalized to pre-treatment levels. F. Representative images of ATP/ADP fluorescent signal intensity (left) and image-based quantitative analysis (right) before and after 5 h of exposure to OM (+OM, closed circles) or drug vehicle (-OM, open circles). Scale bar 100  $\mu\text{m}$ . Data represent the mean  $\pm$  s.e.m.; n = 5 (A), 5 (B), 10 (C), 6–15 (E) and 6 (F) experimental chip replicate \*  $P < 0.05$ , \*\*  $P < 0.01$ , \*\*\*  $P < 0.001$ , \*\*\*\*  $P < 0.0001$ . Red arrow indicates the end of EGTA or OM treatment in A, B, and E.

impedance 3 h post-treatment but it recovered to baseline pre-treatment levels 3 days after OM removal (Fig. 4E). Using fluorescent reporters indicating ATP/ADP metabolic activity and cell viability, we observed >12% drop in the ATP/ADP signal ratio at 5 h and >14% drop in cell viability at 3 h after treatment compared to control chips (Fig. 4F, Supplementary Fig. S4D). These findings are consistent with past studies that showed OM produces a similar decrease in oxygen consumption in Huh7 cells (Theurey et al., 2016; Turcios et al., 2019; Zeidler et al., 2017) as well as in endothelial cells (Patella et al., 2015). In the Huh7 cells, OM also has been shown to reduce cell proliferation and increase cell death (Nwosu et al., 2018). This is consistent with our finding that OM treatment resulted in decreases in tissue barrier function and anaerobic respiration, as well as an increase in the DNA damage and cell viability in the Liver siChips. Moreover, this decrease in proliferation and oxygen consumption was mirrored by a significant drop in metabolic activity evidenced by a decreased ATP/ADP ratio in OM-treated

chips. Interestingly, the Liver siChip impedance recovered after 5 h of exposure while the oxygen tension continued to increase, which in combination may suggest that inhibition of mitochondrial respiration induces compensatory activities in cells to maintain monolayer and barrier integrity; however, confirming of this hypothesis will require future studies.

Previous reports of microfluidic organ chip devices with integrated electrical, electrochemical, and optical sensors (An et al., 2019; Azizgolshani et al., 2021; Fuchs et al., 2021; Henry et al., 2017; Jalili-Firoozinezhad et al., 2019; Li et al., 2017; Lind et al., 2017; Maoz et al., 2017; Müller et al., 2021; Odijk et al., 2015; Riahi et al., 2016; van der Helm et al., 2019; Zhang et al., 2017) have shown their potential value for different tissue monitoring applications. However, these past studies offered limited on-chip analytical sensing capabilities, had complicated designs that impeded multiplexing and automation, or lacked integration of biomechanical cues such as flow for physiological modeling of 3D

tissue structure and function. Our siChip system with integrated, multifunctional, and analytical sensors tackled these challenges by incorporating electrical, chemical, cellular, and optical sensing and monitoring capabilities for continuous non-invasive measurement of TEER, oxygen tension, pH, cell phenotype and metabolic activities in one device while enabling simultaneous live optical imaging of the chip through the entire duration of the culture. In addition, it allows for easy and reproducible fabrication, scale-up, and multiplexing, while being compatible with a commercially available automated Organ Chip culture instrument. The siChip technology can enable establishment and maintenance of tissue microenvironments with physiological oxygen tension levels, and facilitate more comprehensive studies to improve our understanding of human tissue and organ physiology and disease states.

However, the current system has room for improvement in several areas. While we successfully demonstrated remote monitoring of TEER and metabolic activity, oxygen and pH measurements required on-site presence. Integrating optical microdetectors into the mTray could enable remote monitoring of all parameters that could overcome this limitation in future versions of the system. Although the Zoë™ Culture Module was used here as the host operating system, it might not be ideal for large-scale industrial use. However, our chip design provides flexibility to adapt to higher throughput systems. Additionally, exploring alternative materials and manufacturing processes could further streamline production. This study utilized cancer cell lines to validate the system, future studies are encouraged to use primary human cells from healthy and disease donors to explore the systems' potential to provide greater clinically relevance.

#### 4. Conclusion

Here we presented a multi-sensor integrated Organ Chip (siChip) system that provides a robust platform for continuous and simultaneous measurement of different metabolic functions *in vitro*, as demonstrated in human Gut and Liver siChip over extended culture times. We showed that the siChip design made of both PC and PDMS materials allows us to recapitulate *in vivo*-like morphological, oxygen tension, metabolic, and functional human tissue responses to chemical and bacterial stimuli, while allowing near-continuous analytical measurements of these responses at high temporal resolution. The straightforward and scalable fabrication of siChips, their operation both as standalone system as well as modules that can be cultured using commercially available automated culture instruments, and their inline remote data collecting interfaces facilitate their applicability for drug and therapeutic development and testing with clinically relevant reproducibility and reliability.

#### CRediT authorship contribution statement

**Zohreh Izadifar:** Writing – review & editing, Writing – original draft, Visualization, Validation, Resources, Methodology, Investigation, Formal analysis, Data curation, Conceptualization. **Berenice Charrez:** Writing – review & editing, Writing – original draft, Visualization, Resources, Investigation, Formal analysis, Data curation. **Micaela Almeida:** Visualization, Resources, Methodology, Investigation. **Stijn Robben:** Software, Investigation. **Kanoelani Pilobello:** Visualization, Resources, Investigation. **Janet van der Graaf-Mas:** Software, Investigation. **Susan L. Marquez:** Resources, Methodology. **Thomas C. Ferrante:** Resources, Methodology. **Kostyantyn Shcherbina:** Software. **Russell Gould:** Data curation. **Nina T. LoGrande:** Resources. **Adama M. Sesay:** Writing – review & editing, Supervision, Project administration, Methodology, Conceptualization. **Donald E. Ingber:** Writing – review & editing, Supervision, Funding acquisition, Conceptualization.

#### Declaration of competing interest

Donald E. Ingber is a founder, board member and Scientific Advisory

Board chair of, and holds equity in, Emulate Inc. The remaining authors declare no competing interests.

#### Data availability

Data will be made available on request.

#### Acknowledgment

We acknowledge research funding from the Bill and Melinda Gates Foundation, Seattle, WA (INV-035977 to D.E.I.) and DARPA (W911NF-19-2-0027 to D.E.I.), Natural Science and Engineering Research Council of Canada (NSERC Postdoctoral Fellowship to Z.I.), and support from the Wyss Institute for Biologically Inspired Engineering at Harvard University.

#### Appendix A. Supplementary data

Supplementary data to this article can be found online at <https://doi.org/10.1016/j.bios.2024.116683>.

#### References

- Al-Ani, A., Toms, D., Kondro, D., Thundathil, J., Yu, Y., Ungrin, M., 2018. Oxygenation in cell culture: critical parameters for reproducibility are routinely not reported. *PLoS One* 13 (10), e0204269.
- An, Y., Jin, T., Zhang, F., He, P., 2019. Electric cell-substrate impedance sensing (ECIS) for profiling cytotoxicity of cigarette smoke. *J. Electroanal. Chem.* 834, 180–186.
- Aoi, W., Marunaka, Y., 2014. Importance of pH homeostasis in metabolic health and diseases: crucial role of membrane proton transport. *BioMed Res. Int.* 2014.
- Auner, A.W., Tasneem, K.M., Markov, D.A., McCawley, L.J., Hutson, M.S., 2019. Chemical-PDMS binding kinetics and implications for bioavailability in microfluidic devices. *Lab Chip* 19 (5), 864–874.
- Azizgolshani, H., Coppeta, J.R., Vedula, E.M., Marr, E.E., Cain, B.P., Luu, R.J., Lech, M.P., Kann, S.H., Mulhern, T.J., Tandon, V., Tan, K., Haroutunian, N.J., Keegan, P., Rogers, M., Gard, A.L., Baldwin, K.B., de Souza, J.C., Hoefler, B.C., Bale, S.S., Kratchman, L.B., Zorn, A., Patterson, A., Kim, E.S., Petrie, T.A., Wiertel, E.L., Williams, C., Isenberg, B.C., Charest, J.L., 2021. High-throughput organ-on-chip platform with integrated programmable fluid flow and real-time sensing for complex tissue models in drug development workflows. *Lab Chip* 21 (8), 1454–1474.
- Baracu, A.M., Dinu Gugoasa, L.A., 2021. Review—recent advances in microfabrication, design and applications of amperometric sensors and biosensors. *J. Electrochem. Soc.* 168 (3), 037503.
- Berg, J., Hung, Y.P., Yellen, G., 2009. A genetically encoded fluorescent reporter of ATP: ADP ratio. *Nat. Methods* 6 (2), 161–166.
- Berger, E., Vega, N., Weiss-Gayet, M., Gélócn, A., 2015. Gene network analysis of glucose linked signaling pathways and their role in human hepatocellular carcinoma cell growth and survival in HuH7 and HepG2 cell lines. *BioMed Res. Int.* 2015.
- Bulutoglu, B., Rey-Bedón, C., Mert, S., Tian, L., Jang, Y.Y., Yarmush, M.L., Usta, O.B., 2020. A comparison of hepato-cellular *in vitro* platforms to study CYP3A4 induction. *PLoS One* 15 (2), e0229106.
- Bussooa, A., Tubbs, E., Revol-Cavalier, F., Chmayssem, A., Alessio, M., Cosnier, M.-L., Verplanck, N., 2022. Real-time monitoring of oxygen levels within thermoplastic Organ-on-Chip devices. *Biosens. Bioelectron.* X 11, 100198.
- Byrne, M.B., Leslie, M.T., Gaskins, H.R., Kenis, P.J., 2014. Methods to study the tumor microenvironment under controlled oxygen conditions. *Trends Biotechnol.* 32 (11), 556–563.
- Carreau, A., Hafny-Rahbi, B.E., Matejuk, A., Grillon, C., Kieda, C., 2011. Why is the partial oxygen pressure of human tissues a crucial parameter? Small molecules and hypoxia. *J. Cell Mol. Med.* 15 (6), 1239–1253.
- Chauhan, N., Saxena, K., Tikadar, M., Jain, U., 2021. Recent advances in the design of biosensors based on novel nanomaterials: an insight. *Nanotechnology and Precision Engineering* 4 (4), 045003.
- Chen, C.S., Mrksich, M., Huang, S., Whitesides, G.M., Ingber, D.E., 1997. Geometric control of cell life and death. *Science* 276 (5317), 1425–1428.
- Espinosa, M., 2002. Acidic pH and increasing [Ca<sup>2+</sup>] reduce the swelling of mucins in primary cultures of human cervical cells, 17 (8), 1964–1972.
- Farooqi, H.M.U., Kang, B., Khalid, M.A.U., Salih, A.R.C., Hyun, K., Park, S.H., Huh, D., Choi, K.H., 2021. Real-time monitoring of liver fibrosis through embedded sensors in a microphysiological system. *Nano Convergence* 8 (1), 1–12.
- Ferrari, E., Palma, C., Vesentini, S., Occhetta, P., Rasponi, M., 2020. Integrating biosensors in organs-on-chip devices: a perspective on current strategies to monitor microphysiological systems. *Biosensors* 10 (9).
- Fuchs, S., Johansson, S., Tjell, A.Ø., Werr, G., Mayr, T., Tenje, M., 2021. In-line analysis of organ-on-chip systems with sensors: integration, fabrication, challenges, and potential. *ACS Biomater. Sci. Eng.* 7 (7), 2926–2948.
- Gan, E.S., Ooi, E.E., 2020. Oxygen: viral friend or foe? *Virol. J.* 17 (1), 115.
- González-Sánchez, P., Pla-Martín, D., Martínez-Valero, P., Rueda, C.B., Calpena, E., Del Arco, A., Palau, F., Satrústegui, J., 2017. CMT-linked loss-of-function mutations in

- GDAP1 impair store-operated Ca<sup>2+</sup> entry-stimulated respiration. *Sci. Rep.* 7 (1), 1–12.
- Grant, J., Lee, E., Almeida, M., Kim, S., LoGrande, N., Goyal, G., Sesay, A.M., Breaud, D. T., Prantil-Baun, R., Ingber, D.E., 2022. Establishment of physiologically relevant oxygen gradients in microfluidic organ chips. *Lab Chip* 22 (8), 1584–1593.
- Guo, R., Xu, X., Lu, Y., Xie, X., 2017. Physiological oxygen tension reduces hepatocyte dedifferentiation in vitro culture. *Sci. Rep.* 7 (1), 5923.
- Hackett, A., Trinick, R., Rose, K., Flanagan, B., McNamara, P., 2016. Weakly acidic pH reduces inflammatory cytokine expression in airway epithelial cells. *Respir. Res.* 17 (1), 82.
- Hao, W., Chang, C.-P.B., Tsao, C.-C., Xu, J., 2010. Oligomycin-induced bioenergetic adaptation in cancer cells with heterogeneous bioenergetic organization. *J. Biol. Chem.* 285 (17), 12647–12654.
- He, G., Shankar, R.A., Chzhan, M., Samouilov, A., Kuppusamy, P., Zweier, J.L., 1999. Noninvasive measurement of anatomic structure and intraluminal oxygenation in the gastrointestinal tract of living mice with spatial and spectral EPR imaging. *Proc. Natl. Acad. Sci. USA* 96 (8), 4586–4591.
- Hendriks, K.D.W., Brüggewirth, I.M.A., Maassen, H., Gerding, A., Bakker, B., Porte, R.J., Henning, R.H., Leuvenink, H.G.D., 2019. Renal temperature reduction progressively favors mitochondrial ROS production over respiration in hypothermic kidney preservation. *J. Transl. Med.* 17 (1), 265.
- Henry, O.Y.F., Villenave, R., Cronce, M.J., Leineweber, W.D., Benz, M.A., Ingber, D.E., 2017. Organs-on-chips with integrated electrodes for trans-epithelial electrical resistance (TEER) measurements of human epithelial barrier function. *Lab Chip* 17 (13), 2264–2271.
- Hugenholz, J., Perdon, L., Abee, T., 1993. Growth and energy generation by *Lactococcus lactis* subsp. *lactis* biovar diacetylactis during citrate metabolism. *Appl. Environ. Microbiol.* 59 (12), 4216–4222.
- Huh, D., Kim, H.J., Fraser, J.P., Shea, D.E., Khan, M., Bahinski, A., Hamilton, G.A., Ingber, D.E., 2013. Microfabrication of human organs-on-chips. *Nat. Protoc.* 8 (11), 2135–2157.
- Huh, D., Matthews, B.D., Mammoto, A., Montoya-Zavala, M., Hsin, H.Y., Ingber, D.E., 2010. Reconstituting organ-level lung functions on a chip. *Science* 328 (5986), 1662–1668.
- Ingber, D.E., 2022. Human organs-on-chips for disease modelling, drug development and personalized medicine. *Nat Rev Genet* 23, 467–491. <https://doi.org/10.1038/s41576-022-00466-9>.
- Jalili-Firoozinezhad, S., Gazzaniga, F.S., Calamari, E.L., Camacho, D.M., Fadel, C.W., Bein, A., Swenor, B., Nestor, B., Cronce, M.J., Tovaglieri, A., Levy, O., Gregory, K.E., Breaud, D.T., Cabral, J.M.S., Kasper, D.L., Novak, R., Ingber, D.E., 2019. A complex human gut microbiome cultured in an anaerobic intestine-on-a-chip. *Nat. Biomed. Eng.* 3 (7), 520–531.
- JanssenDuijghuijsen, L.M., Grefte, S., de Boer, V.C.J., Zeper, L., van Dartel, D.A.M., van der Stelt, I., Bekkenkamp-Grovenstein, M., van Norren, K., Wichers, H.J., Keijzer, J., 2017. Mitochondrial ATP depletion disrupts caco-2 monolayer integrity and internalizes claudin 7. *Front. Physiol.* 8.
- Johannsen, D.L., Ravussin, E., 2009. The role of mitochondria in health and disease. *Curr. Opin. Pharmacol.* 9 (6), 780–786.
- Kawamoto, M., Yamaji, T., Saito, K., Shirasago, Y., Satomura, K., Endo, T., Fukasawa, M., Hanada, K., Osada, N., 2020. Identification of characteristic genomic markers in human hepatoma Huh-7 and Huh7. 5.1-8 cell lines. *Front. Genet.* 11, 546106.
- Kim, H.J., Huh, D., Hamilton, G., Ingber, D.E., 2012. Human gut-on-a-chip inhabited by microbial flora that experiences intestinal peristalsis-like motions and flow. *Lab Chip* 12, 2165–2174.
- Kulsharova, G., Kurmangaliyeva, A., Darbayeva, E., Rojas-Solórzano, L., Toxeitova, G., 2021. Development of a hybrid polymer-based microfluidic platform for culturing hepatocytes towards liver-on-a-chip applications. *Polymers* 13 (19), 3215.
- Kvietys, P.R., Harper, S.L., Korhuis, R.J., Granger, D.N., 1985. Effects of temperature on ileal blood flow and oxygenation. *Am. J. Physiol.* 249 (2 Pt 1), G246–G249.
- Lee-Montiel, F.T., Laemmle, A., Dumont, L., Lee, C.S., Huebsch, N., Charwat, V., Okochi, H., Hancock, M.J., Siemons, B., Boggess, S.C., 2020. Integrated hiPSC-Based Liver and Heart Microphysiological Systems Predict Unsafe Drug-Drug Interaction. *BioRxiv*.
- Lee, O., O'Brien, P., 2010. Modifications of mitochondrial function by toxicants. *Comprehensive toxicology* 1, 411–445.
- Li, X., Soler, M., Özdemir, C.I., Belushkin, A., Yesilköy, F., Altug, H., 2017. Plasmonic nanohole array biosensor for label-free and real-time analysis of live cell secretion. *Lab Chip* 17 (13), 2208–2217.
- Lind, J.U., Yadid, M., Perkins, I., O'Connor, B.B., Eweje, F., Chantre, C.O., Hemphill, M. A., Yuan, H., Campbell, P.H., Vlassak, J.J., Parker, K.K., 2017. Cardiac microphysiological devices with flexible thin-film sensors for higher-throughput drug screening. *Lab Chip* 17 (21), 3692–3703.
- Lykke, M.R., Becher, N., Haahr, T., Boedtker, E., Jensen, J.S., Ulbjerg, N., 2021. Vaginal, cervical and uterine pH in women with normal and abnormal vaginal microbiota. *Pathogens* 10 (2).
- Maoz, B.M., Herland, A., Henry, O.Y.F., Leineweber, W.D., Yadid, M., Doyle, J., Mannix, R., Kujala, V.J., FitzGerald, E.A., Parker, K.K., Ingber, D.E., 2017. Organs-on-chips with combined multi-electrode array and transepithelial electrical resistance measurement capabilities. *Lab Chip* 17 (13), 2294–2302.
- Masola, B., Evered, D.F., 1984. Preparation of rat enterocyte mitochondria. *Biochem. J.* 218 (2), 441–447.
- McClelland, G.B., 2011. TISSUE RESPIRATION | cellular respiration. In: Farrell, A.P. (Ed.), *Encyclopedia of Fish Physiology*. Academic Press, San Diego, pp. 951–958.
- Mehta, G., Lee, J., Cha, W., Tung, Y.-C., Linderman, J.J., Takayama, S., 2009. Hard top soft bottom microfluidic devices for cell culture and chemical analysis. *Anal. Chem.* 81 (10), 3714–3722.
- Menon, N.V., Chuah, Y.J., Cao, B., Lim, M., Kang, Y., 2014. A microfluidic co-culture system to monitor tumor-stromal interactions on a chip. *Biomicrofluidics* 8 (6), 064118.
- Modica, T.M.E., Dituri, F., Mancarella, S., Pisano, C., Fabregat, I., Giannelli, G., 2019. Calcium regulates HCC proliferation as well as EGFR recycling/degradation and could be a new therapeutic target in HCC. *Cancers* 11 (10), 1588.
- Morgan, K., Gamal, W., Samuel, K., Morley, S.D., Hayes, P.C., Bagnaninchi, P., Plevris, J. N., 2019. Application of impedance-based techniques in hepatology research. *J. Clin. Med.* 9 (1), 50.
- Müller, B., Sulzer, P., Walch, M., Zirath, H., Buryška, T., Rothbauer, M., Ertl, P., Mayr, T., 2021. Measurement of respiration and acidification rates of mammalian cells in thermoplastic microfluidic devices. *Sensor. Actuator. B Chem.* 334, 129664.
- Nakano, F.Y., Leão, R.d.B.F., Esteves, S.C., 2015. Insights into the role of cervical mucus and vaginal pH in unexplained infertility. *Med. Dent. J.* 2 (2), 1–8.
- Nwosu, Z.C., Battello, N., Rothley, M., Piorońska, W., Sitek, B., Ebert, M.P., Hofmann, U., Sleeman, J., Wöfl, S., Meyer, C., 2018. Liver cancer cell lines distinctly mimic the metabolic gene expression pattern of the corresponding human tumours. *J. Exp. Clin. Cancer Res.* 37 (1), 1–15.
- Odijk, M., van der Meer, A.D., Levner, D., Kim, H.J., van der Helm, M.W., Segerink, L.I., Frimat, J.P., Hamilton, G.A., Ingber, D.E., van den Berg, A., 2015. Measuring direct current trans-epithelial electrical resistance in organ-on-a-chip microsystems. *Lab Chip* 15 (3), 745–752.
- Patella, F., Schug, Z.T., Persi, E., Neilson, L.J., Erami, Z., Avanzato, D., Maione, F., Hernandez-Fernaud, J.R., Mackay, G., Zheng, L., 2015. Proteomics-based metabolic modeling reveals that fatty acid oxidation (FAO) controls endothelial cell (EC) permeability\*[S]. *Mol. Cell. Proteomics* 14 (3), 621–634.
- Perdikis, D.A., Davies, R., Zhuravkov, A., Brenner, B., Etter, L., Basson, M.D., 1998. Differential effects of mucosal pH on human (Caco-2) intestinal epithelial cell motility, proliferation, and differentiation. *Dig. Dis. Sci.* 43 (7), 1537–1546.
- Pfeiffer, S.A., Borisov, S.M., Nagl, S., 2017. In-line monitoring of pH and oxygen during enzymatic reactions in off-the-shelf all-glass microreactors using integrated luminescent microsensors. *Microchim. Acta* 184 (2), 621–626.
- Plesniarski, A., Siddiq, A.B., Su, R.-C., 2021. The microbiome as a key regulator of female genital tract barrier function. *Front. Cell. Infect. Microbiol.* 11.
- Riahi, R., Shaegh, S.A.M., Ghaderi, M., Zhang, Y.S., Shin, S.R., Aleman, J., Massa, S., Kim, D., Dokmeci, M.R., Khademhosseini, A., 2016. Automated microfluidic platform of bead-based electrochemical immunosensor integrated with bioreactor for continual monitoring of cell secreted biomarkers. *Sci. Rep.* 6, 24598–24598.
- Rother-Rutishauser, B., Riesen, F.K., Braun, A., Günther, M., Wunderli-Allenspach, H., 2002. Dynamics of tight and adherens junctions under EGTA treatment. *J. Membr. Biol.* 188 (2), 151–162.
- Ruas, J.S., Siqueira-Santos, E.S., Amigo, I., Rodrigues-Silva, E., Kowaltowski, A.J., Castilho, R.F., 2016. Underestimation of the maximal capacity of the mitochondrial electron transport system in oligomycin-treated cells. *PLoS One* 11 (3), e0150967.
- Samak, G., Narayanan, D., Jaggar, J.H., Rao, R., 2011. CaV1.3 channels and intracellular calcium mediate osmotic stress-induced N-terminal c-Jun kinase activation and disruption of tight junctions in Caco-2 CELL MONOLAYERS. *J. Biol. Chem.* 286 (34), 30232–30243.
- Selli, C., Erac, Y., Kosova, B., Erdal, E.S., Tosun, M., 2015. Silencing of TRPC1 regulates store-operated calcium entry and proliferation in Huh7 hepatocellular carcinoma cells. *Biomed. Pharmacother.* 71, 194–200.
- Shin, W., Wu, A., Massidda, M.W., Foster, C., Thomas, N., Lee, D.-W., Koh, H., Ju, Y., Kim, J., Kim, H.J., 2019. A robust longitudinal Co-culture of obligate anaerobic gut microbiome with human intestinal epithelium in an anoxic-oxic interface-on-a-chip. *Front. Bioeng. Biotechnol.* 7.
- Sivertsson, L., Ek, M., Darnell, M., Edebert, I., Ingelman-Sundberg, M., Neve, E.P., 2010. CYP3A4 catalytic activity is induced in confluent Huh7 hepatoma cells. *Drug Metab. Dispos.* 38 (6), 995–1002.
- Srinivasan, B., Kolli, A.R., Esch, M.B., Abaci, H.E., Shuler, M.L., Hickman, J.J., 2015. TEER measurement techniques for in vitro barrier model systems. *J. Lab. Autom.* 20 (2), 107–126.
- Theurey, P., Tubbs, E., Vial, G., Jacquemetton, J., Bendridi, N., Chauvin, M.-A., Alam, M. R., Le Romancer, M., Vidal, H., Rieussel, J., 2016. Mitochondria-associated endoplasmic reticulum membranes allow adaptation of mitochondrial metabolism to glucose availability in the liver. *J. Mol. Cell Biol.* 8 (2), 129–143.
- Toepke, M.W., Beebe, D.J., 2006. PDMS absorption of small molecules and consequences in microfluidic applications. *Lab Chip* 6 (12), 1484–1486.
- Trepiana, J., Meijide, S., Navarro, R., Hernández, M.L., Ruiz-Sanz, J.I., Ruiz-Larrea, M.B., 2017. Influence of oxygen partial pressure on the characteristics of human hepatocarcinoma cells. *Redox Biol.* 12, 103–113.
- Turcios, L., Chacon, E., Garcia, C., Eman, P., Cornea, V., Jiang, J., Spear, B., Liu, C., Watt, D.S., Marti, F., 2019. Autophagic flux modulation by Wnt/ $\beta$ -catenin pathway inhibition in hepatocellular carcinoma. *PLoS One* 14 (2), e0212538.
- van der Helm, M.W., Henry, O.Y.F., Bein, A., Hamkins-Indik, T., Cronce, M.J., Leineweber, W.D., Odijk, M., van der Meer, A.D., Eijkkel, J.C.T., Ingber, D.E., van den Berg, A., Segerink, L.I., 2019. Non-invasive sensing of transepithelial barrier function and tissue differentiation in organs-on-chips using impedance spectroscopy. *Lab Chip* 19 (3), 452–463.
- Varadarajan, S., Stephenson, R.E., Miller, A.L., 2019. Multiscale dynamics of tight junction remodeling. *J. Cell Sci.* 132 (22).

- Yang, N., Tang, Y., Wang, F., Zhang, H., Xu, D., Shen, Y., Sun, S., Yang, G., 2013. Blockade of store-operated Ca<sup>2+</sup> entry inhibits hepatocarcinoma cell migration and invasion by regulating focal adhesion turnover. *Cancer Lett.* 330 (2), 163–169.
- Zeidler, J.D., Fernandes-Siqueira, L.O., Carvalho, A.S., Cararo-Lopes, E., Dias, M.H., Ketzer, L.A., Galina, A., Da Poian, A.T., 2017. Short-term starvation is a strategy to unravel the cellular capacity of oxidizing specific exogenous/endogenous substrates in mitochondria. *J. Biol. Chem.* 292 (34), 14176–14187.
- Zhang, Y.S., Aleman, J., Shin, S.R., Kilic, T., Kim, D., Mousavi Shaegh, S.A., Massa, S., Riahi, R., Chae, S., Hu, N., Avci, H., Zhang, W., Silvestri, A., Sanati Nezhad, A., Manbohi, A., De Ferrari, F., Polini, A., Calzone, G., Shaikh, N., Alerasool, P., Budina, E., Kang, J., Bhise, N., Ribas, J., Pourmand, A., Skardal, A., Shupe, T., Bishop, C.E., Dokmeci, M.R., Atala, A., Khademhosseini, A., 2017. Multisensor-integrated organs-on-chips platform for automated and continual in situ monitoring of organoid behaviors. *Proc. Natl. Acad. Sci. USA* 114 (12), E2293–E2302.